Research Article

Cancer Immunology Research

Exosomes Released from Tumor-Associated Macrophages Transfer miRNAs That Induce a Treg/Th17 Cell Imbalance in Epithelial Ovarian Cancer

Jieru Zhou[1], Xiaoduan Li[2], Xiaoli Wu[1], Ting Zhang[3], Qinyi Zhu[2], Xinjing Wang[1], Husheng Wang[1], Kai Wang[2], Yingying Lin[4], and Xipeng Wang[1]

Abstract

The immune microenvironment is crucial for epithelial ovarian cancer (EOC) progression and consists of tumor-associated macrophages (TAM) and T lymphocytes, such as regulatory T cells (Treg) and T helper 17 (Th17) cells. In this study, the Treg/Th17 ratio was significantly higher in EOC *in situ* and in metastatic peritoneal tissues than in benign ovarian tumors and benign peritoneum. The Treg/Th17 ratio was associated with histologic grade and was an independent prognostic factor for overall survival of EOC patients. On the basis of microarray analysis of exosomes derived from TAMs, we identified miRNAs enriched in the exosomes, including miR-29a-3p and miR-21-5p. When the two miRNA mimics were transfected into $CD4^+$ T cells, they directly suppressed STAT3 and regulated Treg/Th17 cells, inducing an imbalance, and they had a synergistic effect on STAT3 inhibition. Taken together, these results indicate that exosomes mediate the interaction between TAMs and T cells, generating an immune-suppressive microenvironment that facilitates EOC progression and metastasis. These findings suggest that targeting these exosomes or their associated miRNAs might pave the way for the development of novel treatments for EOC. *Cancer Immunol Res; 6(12); 1578–92. ©2018 AACR.*

Introduction

Epithelial ovarian cancer (EOC), the most common cause of gynecologic cancer-related mortality, is characterized by high recurrence and a lack of effective treatments (1). Unlike other solid tumors, EOC cells metastasize to the peritoneal cavity by forming numerous nodules, which is the main obstacle for EOC treatment. An immunosuppressive microenvironment is found in the peritoneum of EOC patients, which further exacerbates tumor progression (2). Our previous studies have shown that the peritoneum of EOC patients contains abundant immune cells, 70% of which are tumor-associated macrophages (TAM) and 25% are T cells (3). TAMs could promote tumor progression by secreting IL10 to increase the frequency of regulatory T cells (Treg; ref. 4), thus illustrating that the mechanisms of cross-talk between tumor-associated immune cells and reversion of the immunosuppressive microenvironment might be an effective strategy for EOC therapy.

TAMs comprise a large proportion of the immune cells in the cancer microenvironment and play significant roles in tumor growth, invasion, angiogenesis, and metastasis (5), and TAM patterns influence long-term outcomes in ovarian cancer patients (6). Generally, TAMs are considered M2-like with an anti-inflammatory and protumor phenotype (7). Some studies have found that M2-like TAMs play an important role in remodeling the tumor microenvironment (TME) by suppressing the adaptive immune response (8). Other studies have demonstrated that TAMs are able to produce exosomes, which are membranous vesicles of endogenic origin, ranging in size from 30 to 100 nm that shuttle biomaterials to adjacent cells within the microenvironment (9, 10). Exosomes have been found to be key players in intercellular communication through horizontal transfer of information via their cargo, which includes proteins, DNA, mRNAs, and miRNAs (11, 12). Exosome-mediated transfer of mRNAs and miRNAs is a mechanism of genetic exchange between cells (13). However, the functions of TAM-derived exosomes in the EOC-immunosuppressive microenvironment remain unknown.

T cells in the TME show less antitumor ability and exhibit an immunosuppressive profile (14). Tregs and T helper 17 (Th17) cells are two subsets of $CD4^+$ T cells. Tregs are known as suppressor T cells and are a subpopulation of T cells that maintain tolerance to self-antigen, modulate the immune system, and abrogate autoimmune disease (15, 16). Th17 cells are $CD4^+$ T helper lymphocytes that secrete IL17A and express the

[1]Department of Obstetrics and Gynaecology, XinHua Hospital Affiliated to Shanghai Jiao Tong University School of Medicine, Shanghai, China. [2]Department of Gynecology, Shanghai First Maternity and Infant Hospital, Tongji University School of Medicine, Shanghai, China. [3]Center for Reproductive Medicine, Shanghai Key Laboratory for Assisted Reproduction and Reproductive Genetics, Renji Hospital, School of Medicine, Shanghai JiaoTong University, Shanghai, China. [4]Department of Neurosurgery, RenJi Hospital, Shanghai JiaoTong University School of Medicine, Shanghai, China.

Note: Supplementary data for this article are available at Cancer Immunology Research Online (http://cancerimmunolres.aacrjournals.org/).

J. Zhou, X. Li, and X. Wu contributed equally to this article.

Corresponding Authors: Xipeng Wang, Xinhua Hospital Affiliated to Shanghai Jiao Tong University School of Medicine, Department of Obstetrics and Gynecology, XinHua Hospital Affiliated to Shanghai Jiao Tong University School of Medicine, 1665 Kongjiang RD, Yangpu district, Shanghai, 200092, China. Phone: 86-13817806602; E-mail: wangxipeng@xinhuamed.com.cn; and Yingying Lin, Phone: 86-15800727180; Fax: 86-21-68383982; E-mail: yylin@sibs.ac.cn

doi: 10.1158/2326-6066.CIR-17-0479

transcription factor RORγt, which regulates the activation of cytotoxic $CD8^+$ T cells (11, 16).

A Treg/Th17 cell imbalance characterizes many diseases, such as human systemic lupus, diabetes, and some tumors (17–19). Tregs and Th17 cells share a reciprocal differentiation pathway from uncommitted $CD4^+$ precursors (12). However, little is known about the mechanisms affecting the imbalance between Tregs and Th17 cells in the TME, especially in EOC. In this study, we investigated the imbalance between Tregs and Th17 cells in EOC patients and its clinical implications. Both *in vitro* and *in vivo* studies showed that the imbalance between Tregs and Th17 cells drove EOC progression and metastasis. We further illustrated the communication between TAMs and T lymphocytes in the TME of EOC.

In addition, we showed that TAM-derived exosomes transferred miRNAs, including miR-29a-3p and miR-21-5p, to synergistically induce the Treg/Th17 cell imbalance through direct targeting of STAT3 in $CD4^+$ T cells. This study reveals a functional mechanism of TAMs in EOC progression. Targeting these exosomes or associated miRNAs might serve as a therapeutic strategy for EOC treatment.

Materials and Methods

Patients and specimens

Patients and healthy donors were included from Shanghai First Maternity and Infant Hospital, Tongji University School of Medicine, Shanghai, China. Specimens included peripheral blood (PB), ascites, benign ovarian tumors, EOC tissue, benign peritoneum, and EOC peritoneum. PB was obtained from 150 patients and 20 healthy donors, and ascites came from 27 EOC patients with ascites. EOC tissues were from 124 EOC patients, 15 of whom had peritoneal tissue collected at the same time. Benign tumor tissues were from 26 benign ovarian tumors patients, 6 of whom had peritoneal tissue collected at the same time. Specimens are stored in the form of both frozen sections and formalin-fixed paraffin-embedded (FFPE) samples. Patients with tumor histories from other systemic sites were excluded, patients with recurrent tumors were excluded, and none of the cancer patients received any chemotherapy before specimens were obtained. EOC patients were divided into two groups according to pathologic diagnosis, thus serous ovarian cancer (SOC) and nonserous ovarian cancer (NSOC). PB was collected preoperatively, and tissue samples and ascites were collected intraoperatively. The objectives and implications of the results were explained, and institutionally approved written informed consent was obtained from each participant. The study protocol was reviewed and approved by the Institutional Review Board of Shanghai First Maternity and Infant Hospital, in accordance with the Declaration of Helsinki.

Cell culture

The mouse EOC cell line ID8 and the human monocyte cell line THP-1 were obtained from Fuheng Bio at 2015 (FuHeng Cell Center; FH1075 and FH0113). The ID8 cells were cultured in high-glucose DMEM (HyClone, SH30243.01B) with 10% fetal bovine serum (FBS, Gibco, 10099141), and THP-1 cells were cultured in RPMI-1640 (HyClone, SH30809.01B) with 10% FBS. Cell lines were maintained in culture for no more than 10 passages. All the cell lines were authenticated using short tandem repeat analysis every 6 months, with the latest test in August 2017. Cells were also authenticated by morphology, phenotype, and growth and routinely screened for *mycoplasma* (Sciencell, Mycoplasma PCR Detection Kit, 8208). Testing for mycoplasma contamination in cell cultures was routinely performed at least every 3 months, with the latest test in November 2017.

Generation of ID8-luciferase cells

ID8 cells were transduced with a lentiviral vector (PHY-024 lentivirus vector) containing a luciferase reporter (GenBank NO:MF693179.1) together with the puromycin resistance gene (ID8-Luc-pur). The production of a third-generation lentivirus was provided by Hanyin Biotechnology Limited Company (Shanghai), and we followed the lentiviral operation manual they provided. First, the ID8 cells were seeded into 6-well plates with the cell density being about 50% by the second day. Next, we obtained MOI (multiplicity of infection) values according to preliminary experiments (MOI = 3–5). The original cell culture medium was then removed, and the lentivirus was added to the cells and incubated overnight. After 24 hours of infection, the culture medium containing the lentivirus was removed and replaced with fresh culture medium. After 72 hours, the transfected cells were grown in complete high-glucose DMEM with puromycin (3 μg/mL; Shanghai MaoKang Biotechnology, MS0011-25MG) for purity screening.

M0, M1, and M2 macrophages and the coculture system

M0/M1/M2 macrophages were derived from human peripheral blood mononuclear cells (PBMC). Fresh human PB $CD14^+$ monocytes and $CD4^+$ T cells were provided by 10 healthy donors and isolated using CD14 microbeads (Miltenyi Biotec, 130-050-201) and CD4 microbeads (Miltenyi Biotec, 130-045-101). M0 macrophages were induced with M-CSF (10 ng/mL; R&D Systems, 416-ML-050). M1 macrophages were induced with M-CSF (10 ng/mL), LPS (500 ng/mL; Sigma, L2880-25MG), and IFNr (20 ng/mL; R&D Systems, 285-IF-100) for 3 days. M2 macrophages were induced with M-CSF (10 ng/mL) and IL4 (20 ng/mL; R&D Systems, 6507-IL-010) for 3 days (20). The control group was untreated. $CD4^+$ T cells (5×10^5) were prestimulated with anti-CD3 (10 μg/mL; BD Pharmingen, 550368) and anti-CD28 (5 μg/mL; BD Pharmingen, 555726) for 3 days. The 5×10^5 T cells were then cocultured with the different macrophages for 3 days, with a T-cell:macrophage ratio of 1:2.

For the coculture exosome and $CD4^+$ T-cell system, after induction of $CD14^+$ monocytes into M1/M2 macrophages, the culture medium was replaced with RPMI-1640. Exosomes were isolated as described below. M1/M2 exosomes (50 μg/mL) were added to 10^5 autologous $CD4^+$ T cells and cocultured for 3 days. The $CD4^+$ T cells were prestimulated with anti-CD3(10 μg/mL) and anti-CD28 (5 μg/mL) for 3 days.

Exosome isolation

THP-1 cells, TAMs, M1 macrophages, and M2 macrophages were cultured in RPMI-1640 for 24 hours. M1 and M2 macrophages were prestimulated as described above. To isolate exosomes, supernatants were centrifuged two times ($1{,}000 \times g$ for 10 minutes and $3{,}000 \times g$ for 30 minutes to remove cells and cellular debris), followed by addition of Total Exosome Isolation Reagent (from cell culture medium; Life Technologies, 4478359) overnight and centrifugation for $10{,}000 \times g$ for1 hour. Exosomes were resuspended in PBS and stored at −80°C. The concentration of exosomes was detected using a BCA Protein Assay Kit (Thermo Scientific, 23225).

Electron microscopy

Exosome pellets were resuspended in PBS and loaded onto a carbon-coated copper electron microscope grid and then stained with 2% uranyl acetate. The exosomes were observed under a Tecnai G2 F20 ST Transmission electron microscope.

Transfection with miRNA mimics

Mimics were purchased from Shanghai GenePharma Co, Ltd., and the human sequences used in the *in vitro* experiment were different from the mouse sequences used in the *in vivo* experiment. The following oligonucleotide sequences aligned to the human strains were 5′ FAM-labeled, and fluorescence was observed following successful transfection. "Hsa" indicates the logogram of homo sapiens, "mmu" indicates the logogram of mus musculus, and "NC" indicates negative control. Hsa-miR-29a-3p mimic: uagcaccaucugaaaucgguua; hsa-miR-21-5p mimic: uagcuuaucagacugauguuga; NC: uucuccgaacgugucacgudtdt. The following oligonucleotide sequences aligned to mouse strains were 5′ FAM-labeled, and fluorescence was observed following successful transfection. NC: uucuccgaacgugucacgutt; mmu-mir-21-5p-mimic: uagcuuaucagacugauguugaaacaucagucugauaagcuauu; mmu-mir-29a-3p mimic: uagcaccaucugaaaucgguuaaccgauuucagauggugcuauu; mmu-mir-21-5p-inhibitor: ucaacaucagucugauaagcua; mmu-mir-29a-3p inhibitor: uaaccgauuucagauggugcua. "Both mimics" indicates that the hmiR-21-5p mimic and miR-29a-3p mimic were used simultaneously, and "both inhibitors" refers to the use of the miR-21-5p inhibitor and the hsa-miR-29a-3p inhibitor.

X-tremeGENE siRNA transfection reagent (Roche, 04476093001) was used to transfer mimics into T cells according to the manufacturer's instructions. For the combination of miR-21-5p and miR-29a-3p, we combined the concentration of the single miRNAs used in the experiments, and thus the overall concentration of miRNAs was doubled. $CD4^+$ T cells (5×10^5) were transfected with 3.5 μg NC, 3.5 μg hsa-miR-21-5p mimic, 3.5 μg hsa-miR-29a-3p mimic, both mimics (3.5 μg hsa-miR-21-5p mimic and 3.5 μg hsa-miR-29a-3p mimic), or both inhibitors (3.5 μg hsa-miR-21-5p inhibitor and 3.5 μg hsa-miR-29a-3p inhibitor). For the *in vivo* experiment, we determined whether the transfection was successful by fluorescence microscope after 6 hours. For the *in vitro* experiment, the five-mimic transfection was determined by real-time PCR after 48 hours or Western blotting after 72 hours.

Western blots

The total proteins were lysed with RIPA (Beyotime, P0013E) and separated on 10% SDS PAGE gels. The gels were then transferred to polyvinylidene fluoride membranes (Millipore, U650617). After blocking with 5% nonfat milk for 1 hour, the membranes were incubated with primary antibody at 4°C overnight. Anti-rabbit IgG (Cell Signaling Technology, 7074S) was used as the secondary antibody. Exosome biomarkers were detected by Western blotting using the following primary antibodies: tetraspanin molecule CD9 (Abcam, Rabbit mAb, ab92716), CD63 (Abcam, Rabbit pAb, ab216130), CD81 (Abcam, Rabbit mAb, ab109201), Tsg 101 molecules (Abcam, Rabbit mAb, ab125011), and GAPDH (CST, Rabbit mAb, 5174).

$CD4^+$ T cells were transfected with NC, hsa-miR-21-5p-mimic, hsa-miR-29a-3p-mimic, both mimics, or both inhibitors, and the cells were also simultaneously lysed in total protein lysis buffer after 72 hours of transfection. Detection of STAT3 and actin was performed with anti-STAT3 (CST, Rabbit mAb, 12640) and anti-β-actin (CST, Rabbit mAb, 8457) via Western blotting. ImageJ was used for grayscale analysis in Western blotting.

Flow-cytometric analysis of T-cell subsets and cytokines in $CD4^+$ T cells

After T-cell coculture with macrophages or exosomes from macrophages, the proportion of Tregs ($CD4^+$ $FoxP3^+$) and Th17 ($CD4^+IL17^+$) cells was detected by flow-cytometric analysis. For IL17 detection, the cells were stimulated with T-cell stimulation cocktail (2 μL/mL; eBioscience, 00-4975-93) for 4 hours before staining. Cells (5×10^5) were used as experimental samples. First, cells were stained with fixable viability stain 780 (fvs780, BD Pharmingen, 565388) for 15 minutes. Cells were stained extracellularly with CD4-Pecy5.5 (eBioscience, 45-0049-42) for 30 minutes at 4°C in the dark. Subsequently, the cells were fixed and permeabilized with Perm/Fix solution (eBioscience) for 45 minutes in the dark and then intracellularly stained with anti-IL17–phycoerythrin (PE, eBioscience, 25-7177-82) and anti-FoxP3–allophycocyanin (APC, eBioscience, 17-4776-42) for 30 minutes at 4°C in the dark. Flow-cytometric analysis was performed using a BD FACSCanto II, and data were analyzed using FlowJo V10.0.

To explore the STAT3 signal downregulation in T-cell subsets after miRNA transduction into native $CD4^+$ T cells, and to detect cytokines from Tregs and Th17 cells by flow-cytometric analysis, NC, hsa-miR-21-5p-mimic, hsa-miR-29a-3p-mimic, both mimics, or both inhibitors were transfected into native $CD4^+$ T cells as described in the "Transfection with miRNA mimics." After 48 hours, the IL17 Secretion Assay, Cell Enrichment and Detection Kit (PE; Miltenyi, 130-094-542) was used to isolate Th17 cells, and the $CD4^+CD25^+$ Regulatory T-Cell Isolation kit (Miltenyi, 130-091-301) was used to isolate Tregs.

According to the cytokine propensity of Tregs and Th17 cells, we used flow cytometry to detect TGFβ, IL10 (21), and IL4 for Tregs (22), and TNFα and IL6 for Th17 cells (23). Similar to the previous experiment, 5×10^5 cells stained with fvs780 for 15 minutes. Cells were also stained extracellularly with CD4-bb515 (BD Pharmingen, 564419) as described above. Subsequently, the cells were fixed and permeabilized for 45 minutes in the dark, and then Tregs were intracellularly stained with anti-TGFβ1–PE (BD Pharmingen, 562339), anti-IL10–APC (BD Pharmingen, 554707), and anti-IL4–PerCP-cy5.5 (BD Pharmingen, 561234) for 30 minutes at 4°C in the dark. At the same time, Th17 cells were stained with anti-TNFα–PE-CY7 (BD Pharmingen, 557647) and anti-IL6–APC (BD Pharmingen, 561441). Flow-cytometric analysis was also performed using BD FACSCanto II. Data were analyzed using FlowJo V10.0.

Confocal microscopy

Detection of Tregs ($CD4^+FoxP3^+$) and Th17 ($CD4^+IL17^+$) cells in frozen sections of benign ovarian tumors, EOC tissue, benign peritoneum, and EOC peritoneum was performed using mouse monoclonal CD4 antibodies (Abcam, ab846), rat polyclonal anti-FoxP3 (Abcam, ab54501), and rabbit polyclonal anti-IL17A (Abcam, ab79056). All cell nuclei were counterstained with DAPI (D9542, Sigma). Alexa Fluor 488–conjugated goat anti-mouse IgG (Jackson, 115-545-205) was used for detection of anti-CD4, Cy3-conjugated goat anti-rat IgG (Jackson, 112-165-003) was used for detection of anti-FoxP3, and Alexa Fluor 647–conjugated anti-rabbit secondary antibody (Jackson,

111-605-003) was used for detection of anti-IL17. Images were taken with a Zeiss LSM 510 laser scanning confocal microscope. Quantitative analysis was performed in five random fields per tumor by counting the number of cells at × 40 magnification.

To detect exosomes derived from macrophages acting on $CD4^+$ T cells, M2 macrophages were derived from PBMCs. M2 macrophages were induced with M-CSF and IL4 as described above. Macrophages (1×10^6) were stained with 500 nmol/L SYTO RNASelect Green Fluorescent Cell Stain [Life Technology, S-32703, Green, ∼490/530 nm) to label RNA, and DiIC16(3); 1:300 dilution; Invitrogen, D384, Red, ∼589/617 nm] was added to label membranes for 20 minutes at 37°C. The medium was removed, and macrophages were washed three times with PBS. RPMI-1640 and 1×10^6 $CD4^+$ T cells were then added. The cells were cultured for 24 hours, and T cells were collected for confocal microscopy to detect macrophage exosomes taken up by T cells. Images were taken with a Zeiss LSM 510 laser scanning confocal microscope.

In vivo experiments

Fresh mouse $CD4^+$ T cells were purified from spleens of C57BL/6 mice (4–6 weeks old, female) with mouse CD4 (L3T4) microbeads (Miltenyi Biotec, 130-049-201) following the manufacturer's instructions. In brief, 10^7 cells were cultured with 40 μL of anti-CD4 beads for 15 minutes protected from light at 4°C and then washed 3 times. Next, the cells were resuspended in 500 μL of buffer, and the cell suspension was applied to an LS column (Miltenyi Biotec, Germany, 130-042-201). The percentage of the $CD4^+$ T cells in total obtained cells was analyzed by flow cytometry. The mouse $CD4^+$ T cells were cultured in complete RPMI-1640 with 10% FBS and 1% penicillin–streptomycin (P/S, Gibco, 15070063) and used within 2 weeks.

To induce a Treg/Th17 imbalance, $CD4^+$ T cells were incubated in a T25 culture flask (5×10^6 cells/flask). The T cells were then divided into three groups. The Treg/Th17-low ratio (ratio = 0.3) group was prestimulated with anti-CD3 (10 μg/mL coated in advance; eBioscience, 16-0031) and anti-CD28 (5 μg/mL; eBioscience, 16-0281). The control group was cultured with complete RPMI-1640 medium for 3 days. The Treg/Th17-high ratio (ratio = 1.7) group was cultured with trichostatin A (5 nmol/L/mL, TSA, Sigma, T8552) for 3 days to induce a Treg/Th17 imbalance (24).

Female C57BL/6 mice (6 weeks of age, 15–17 g) were purchased from Shanghai Slac Laboratory Animal and bred under SPF conditions in Tongji University School, Shanghai, China. The 45 mice were randomly divided into 3 groups and injected intraperitoneally with 0.5 mL of PBS containing 5×10^6 (25, 26) ID8-Luc-pur cells. For the long-term experiments, additional T-cell injections were started 14 days after the first injection in the metastasis model. Each group (control group, Treg/Th17-low group, and Treg/Th17-high group) was administered 0.1 mL of PBS containing 1×10^6 T cells via intraperitoneal injection once a week. The tumors in C57BL/6 mice were examined for Luc expression using D-luciferin (100 mg/kg, Invitrogen, Life Technologies), and images were captured with a NightOWLIILB 983 instrument to assess tumor development every week. Image analyses were carried out with IndiGo software. At the time of sacrifice, ovary, peritoneum, mesentery, and diaphragm were harvested from mice, and specimens are stored as FFPE samples. The experimental endpoint was the time of death due to disease.

Another 50 mice were randomly divided into 5 groups and injected intraperitoneally with 0.5 mL of PBS containing 5×10^6 ID8-Luc-pur cells. $CD4^+$ T cells were transfected with NC, mmu-miR-21-5p mimic, mmu-miR-29a-3p mimic, both mimics, or both inhibitors for 72 hours. For the long-term experiments, additional T cells were injected beginning at 14 days after the first injection in the metastasis model. All groups were injected intraperitoneally with 0.1 mL of PBS containing 1×10^6 T cells once a week. The groups included the NC group, hsa-miR-29a-3p group, hsa-miR-21-5p group, both mimics group, and both inhibitors group. The tumor flux was recorded weekly to observe Luc expression based on D-luciferin to assess tumor development. All the animal experiments were approved by the Medical Animal Care of Tongji University, and the animals were cared for according to the recommended use of laboratory animals. At the time of sacrifice, ovary, mesentery, and diaphragm were harvested and stored as FFPE samples. All peritoneal tissues from the mice were harvested and stored in 4% paraformaldehyde at 4°C. The experimental endpoint was the time of death due to disease.

Agilent miRNA microarray

MiRNA microarray was performed by oeBiotech Limited Company. An Agilent miRNA microarray (8*60K, Design ID: 046064) was used to profile miRNAs in the exosomes released by monocytes (THP-1) and M2 macrophages (GEO number: GSE97467). The M2 macrophages were induced with PMA (50 ng/mL; Sigma, P1585) and IL4 (20 ng/mL), as described above. The culture medium was then replaced with RPMI-1640, and the cells were cultured for 24 hours. Exosomes were isolated as described above. Total RNA was extracted using a mirVanaTM RNA Isolation Kit (Applied Biosystem p/n AM1556), and 100 ng RNA per sample was used on microarray.

Assessment of miRNA expression

$CD14^+$ monocytes were induced to develop into M2 macrophages, and the exosomes from $CD14^+$ monocytes and M2 macrophages were collected. Total RNA from exosomes and T cells was isolated with TRIzol (Invitrogen, Life Technologies, 15596026) and reverse-transcribed into cDNA using a miScript II RT Kit (Qiagen, 218161). Twenty nanogram templates were used, and PCR detection with a miScript SYBR Green PCR Kit (Qiagen, 218073) was performed. The miRNA primers for hsa-miR-146b-5p, hsa-miR-660-5p, hsa-miR-24-3p, hsa-miR-29a-3p, and hsa-miR21-5p were purchased from Shanghai GenePharma Co, Ltd. (Proven custom gene RT-PCR primer kit, F3001). U6 was used as control gene, and the sequences were 5′-CAAGGATGACACGCAAATTCG-3′. The miScript Universal Primer was supplied in a kit. The fold change was calculated as $2^{-\Delta\Delta Ct}$, where $\Delta\Delta Ct = \Delta Ct$ treatment $- \Delta Ct$ control and $\Delta Ct =$ Ct target gene – Ct U6.

Assessment of mRNA expression

To explore the STAT3 signal downregulation in T-cell subsets after the miRNA transduction into native $CD4^+$ T cells, $CD4^+$ T cells were transfected with NC, hsa-miR-21-5p-mimic, hsa-miR-29a-3p-mimic, both mimics, or both inhibitors as described in the "Transfection with miRNA mimics" section. After 48 hours, Th17 cells and Tregs were isolated as stated above. The parent $CD4^+$ T-cell population, Tregs ($CD4^+$ $FoxP3^+$), and Th17 ($CD4^+IL17^+$) cells were also collected for RNA extraction with TRIzol. Total RNA was then reverse-transcribed into cDNA and 20 ng cDNA template used for PCR detection with a PrimeScript RT-PCR kit (Takara,

DRRo14A). The real-time PCR primers used for STAT3 in humans were (F) 5′-CTTTGAGACCGAGGTGTATCACC-3′ and (R) 5′-GGTCAGCATGTTGTACCACAGG-3′ and in mice were (F) 5′-GGGCCATCCTAAGCACAAAG-3′ and (R) 5′- GGTCTTGCCACT-GATGTCCTT -3′. β-Actin primers in humans were (F) 5′-CCTGGCACCCAGCACAAT-3′, (R) 5′-GGGCCGGACTCGTCA-TACT-3′ and in mice were (F) 5′- GTGACGTTGACATCCG-TAAAGA -3′, (R) 5′- GCCGGACTCATCGTACTCC -3′.

The expression of cytokines IL4, IL6, IL10, and TNFα were also detected using real-time PCR. The following primer oligonucleotide sequences were used: IL4, (F) 5′-ATGGGTCT-CACCTCCCAACT-3′ and (R) 5′- GATGTCTGTTACGGTTACG GTCAACTCG-3′; IL6, (F) 5′-ACTCACCTCTTCAGAACGAATTG-3′ and (R) 5′- CCATCTTTGGAAGGTTCAGGTTG-3′; IL10, (F) 5′- GACTTTAAGGGTTACCT GGGTTG-3′ and (R) 5′- TCA-CATGCGCCTTGATGTCTG-3′; TNFα, (F) 5′-CCTC CTCTAAT-CAGCCCTCTG-3′ and (R) 5′-GAGGACCTGGGAGTAGATGAG-3′.The fold change was calculated as $2^{-\Delta\Delta Ct}$, where ΔΔCt = ΔCt treatment − ΔCt control and ΔCt = Ct target gene – Ct β-actin.

Statistical analysis

Statistical analyses were performed with SPSS19.0 software (SPSS Inc.). The data are expressed as the mean ± SEM. All experiments were repeated at least in triplicate. The Mann–Whitney test, univariate analysis of variance (ANOVA, Least-Significant Difference test, LSD test), and Student *t* test were two tailed and used to determine *P* values. Receiver operating characteristic (ROC) analysis was applied to determine optimal sensitivity and specificity of the Treg/Th17 ratio. Overall survival (OS) was calculated using the Kaplan–Meier method to determine the univariate relationship between the Treg/Th17 ratio, age, histologic subtype, and grade. Continuous variables in figures are presented as the mean ± SEM. $P < 0.05$ was considered statistically significant.

For The Cancer Genome Atlas (TCGA) database analysis, the intersection of each top 20% high-expression samples was defined as synergistic high, and the intersection of each bottom 20% low-expression samples was defined as synergistic low to assess the combinational effect of two miRNAs. The Treg/Th17 ratio was calculated from the Treg and Th17 proportions. The top 40% versus bottom 40% for prognosis assessment was chosen. We restricted to the late-stage (III and IV) EOC patients who had evidence of peritoneal invasion. For survival analysis, Kaplan–Meier fitted survival curves were tested for differences using the Mantel–Haenszel test. The corresponding hazards ratios were, respectively, estimated with the Cox regression model.

Study approval

The human studies and animal protocols were approved by the Institutional Review Board of Shanghai First Maternity and Infant Hospital. Written informed consent was obtained from all study participants or their guardians.

Results

Upregulated Treg/Th17 ratios in EOC patients

Ovarian tissue samples from 124 EOC patients and 26 benign ovarian tumor patients were evaluated by immunofluorescence. Tregs were identified as $CD4^+$ $FoxP3^+$, whereas Th17 cells were identified as $CD4^+IL17^+$. Our previous work showed a significantly greater number of Tregs in EOC tissue than in benign tumor tissue (4). In this study, we detected Tregs and Th17 cells in tissue via immunofluorescent staining of frozen sections, including benign ovarian tumors, EOC tissue, benign peritoneum, and EOC peritoneum (Fig. 1A–D). Compared with the ratio for the benign ovarian tumor tissues (1.04 ± 0.25), the Treg/Th17 ratio was significantly higher in EOC patient tumor tissues ($P < 0.001$, Mann–Whitney test; 1.97 ± 0.13; Fig. 1E). The Treg/Th17 ratio was also significantly higher in EOC peritoneal tissues (1.58 ± 0.32) than that in benign peritoneal tissues ($P < 0.001$, Mann–Whitney test; 0.12 ± 0.06; Fig. 1F). Because SOC is a typical representative of EOC and high-grade SOC accounts for 70% to 80% of ovarian cancer deaths, we analyzed the Treg/Th17 ratio in SOC and NSOC, and found that it was significantly higher in the SOC group (2.21 ± 0.19) than in the NSOC group ($P = 0.027$, Mann–Whitney test, 1.65 ± 0.15; Fig. 1G). The Treg/Th17 ratio was also correlated with EOC historical grade (Table 1; and Supplementary Table S1). The Treg percentage was significantly higher in EOC patient blood and ascites than that in other Th17 cells (Supplementary Fig. S1A–S1C). However, no significant difference in the Treg/Th17 ratio in EOC patient blood and ascites was seen (Supplementary Fig. S1D–S1E). Thus, our results indicate that the distribution and ratio of Tregs and Th17 cells in both EOC primary tissue and metastatic peritoneal tissues were significantly higher than those in benign ovarian tumor patients.

Effect of the Treg/Th17 imbalance on growth and metastasis of ovarian cancer

To investigate the influence of the Treg/Th17 imbalance on EOC development, we established a metastasizing ovarian cancer C57BL/6 model with the ID8 cell line to observe ovarian cancer growth and metastasis (25). The ID8 cell line was obtained through spontaneous transformation of normal ovarian surface epithelial cells from C57BL6 mice by repetitive passage *in vitro*. *In vivo*, intraperitoneally injected ID8 cells produce tumors very similar to high-grade SOC (26). *FOXP3* is a special transcription factor in Tregs, and a histone deacetylase (HDAC) inhibitor can alter the histone deacetylation of specific sites in*FOXP3*, specifically, the CpG island, which stabilizes *FOXP3* expression (24). The histone deacetylase (HDAC) inhibitor trichostatin A (TSA) was used to induce a Treg/Th17 imbalance ($P < 0.01$, *t* test; Fig. 2A). Fresh $CD4^+$ T cells were purified from the spleens of C57BL/6 mice, and the $CD4^+$ T-cell purity was nearly 90% (Fig. 2B).

After injection of ID8-Luc-pur cells, we used a bioluminescence imaging system to observe tumor growth every week until death. The fluorescent signal from tumor cells can be detected in organs after tumor cells were injected into the peritoneal cavity of C57BL6 mice (26). The intensity of the bioluminescent signal and the tumor load correlated. Small tumors can be detected by imaging (27). The high Treg/Th17 ratio (ratio = 1.7) group exhibited enhanced tumor load (tumor flux 18280.00 ± 4214.74 cps) at week 11 compared with the control group (tumor flux 4612.80 ± 471.73 cps, $P = 0.002$, *t* test), whereas the low Treg/Th17 ratio (ratio = 0.3) group (tumor flux 2305.80 ± 363.06 cps) showed subdued tumor load ($P = 0.0047$, *t* test; Fig. 2C). Tumor load in the high Treg/Th17 ratio group ($n = 3$) increased more rapidly than in the control group ($P = 0.0125$, *t* test), and the tumor in the low Treg/Th17 ratio group exhibited slower growth than the control group ($P = 0.0031$, *t* test; Fig. 2D). These results were consistent with the cumulative survival rate changes over time. The low Treg/Th17 ratio group showed a longer cumulative survival rate than the control group ($P = 0.033$, log-rank test),

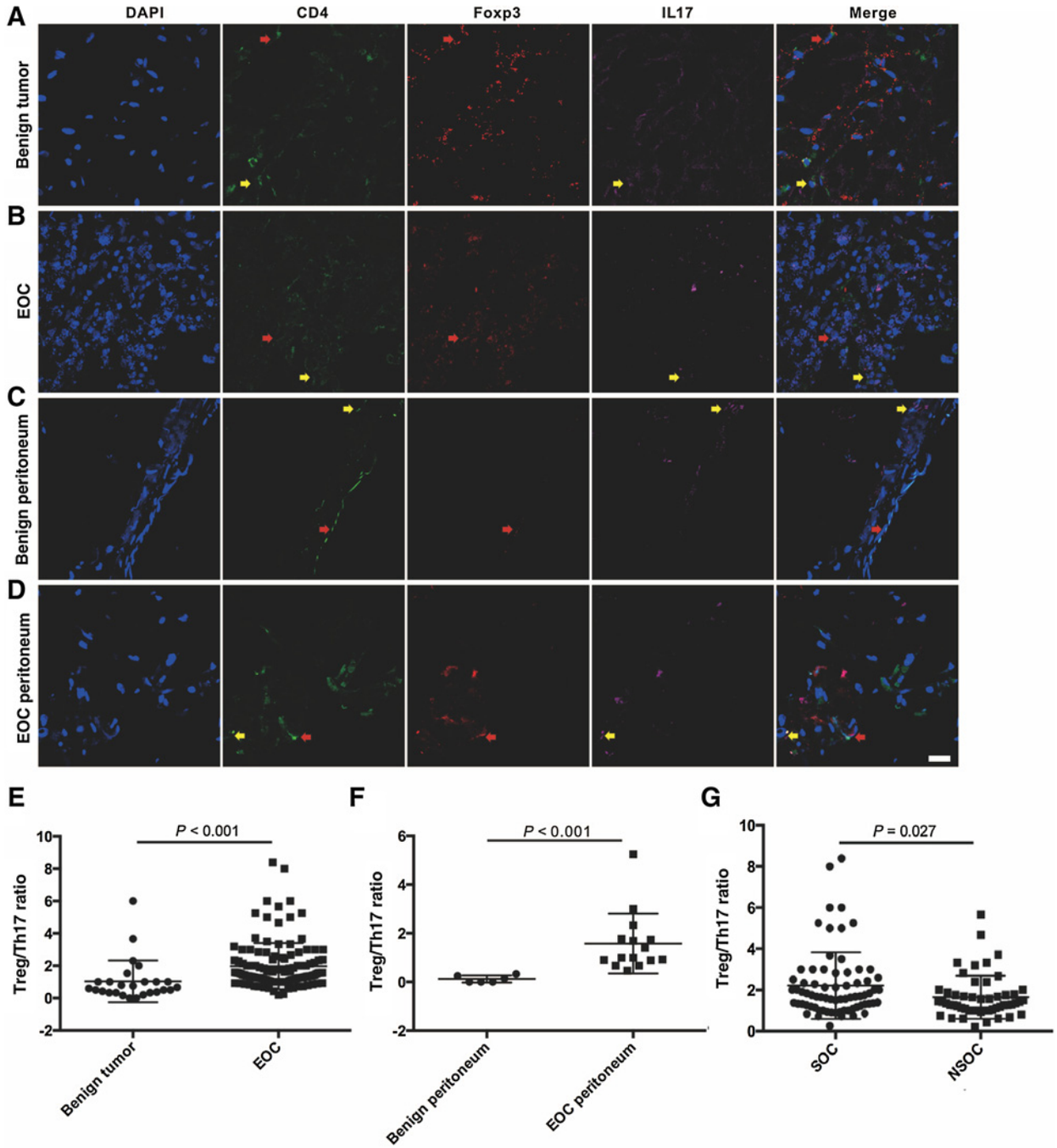

Figure 1.

Distribution of Tregs and Th17 cells in EOC patients. **A** and **B,** Tregs in benign ovarian tumor tissue and in EOC tissue were stained with DAPI (blue, nuclei) and with antibodies targeting CD4 (green) and FoxP3 (red). Th17 cells in benign ovarian tumor tissue and in EOC tissue were stained with DAPI (blue, nuclei) and with antibodies targeting CD4 (green) and IL17 (pink). The mean number of Tregs and Th17 cells was quantified in five high-powered fields (HPF) for each section. **C** and **D,** Tregs in benign peritoneum tissue and in EOC peritoneum tissue were stained with DAPI (blue, nuclei) and with antibodies targeting CD4 (green) and FoxP3 (red). Th17 cells in benign peritoneum tissue and in EOC peritoneum tissue were stained with DAPI (blue, nuclei) and with antibodies targeting CD4 (green) and IL17 (pink). **E,** The Treg/Th17 ratio in EOC tissues ($n = 124$) compared with benign ovarian tumor tissues ($n = 26$). **F,** The Treg/Th17 ratio in EOC peritoneal tissue ($n = 15$) compared with benign peritoneal tissue ($n = 6$). **G,** Treg/Th17 ratio in the SOC ($n = 72$) and NSOC groups ($n = 52$). Scale bar, 50 μm. Results were analyzed via Mann–Whitney test; $P < 0.05$ was considered statistically significant.

Table 1. Association between the Treg/Th17 ratio and clinicopathologic variables in EOC patients

	Ratio < 1.02 *n* (%)	Ratio ≥ 1.02 *n* (%)	Total	*P*
Age				
<50	9 (17.0)	44 (83.0)	53	0.278
≥50	19 (26.8)	52 (73.2)	71	
Histologic subtype				
SOC	14 (19.4)	58 (80.6)	72	0.386
NSOC	14 (26.9)	38 (73.1)	52	
Histologic grade				
Low grade	11 (55.0)	9 (45.0)	20	<0.001
High grade	14 (14.1)	85 (85.9)	99	

and the high Treg/Th17 ratio group had a shorter survival time ($P = 0.037$, log-rank test; Fig. 2E). The tumor flux (cps) was recorded in the three groups every week, and typical images are presented (week 11; Fig. 2F). The peritoneum, mesentery, and diaphragm were harvested from mice and showed greater tumor invasion. Hematoxylin–eosin (H&E) staining confirmed the presence of tumors (Fig. 2G).

After establishing the mouse model, time to tumor formation and metastasis was monitored by living imaging. At the time of sacrifice, tumors were accompanied by metastases throughout the abdominal cavity, especially at peritoneum, mesentery, and diaphragm (Fig. 2G). These experiments demonstrated that an imbalance in the Treg/Th17 ratio affects the growth of tumor cells *in vivo* and that a higher Treg/Th17 ratio promotes ovarian cancer metastasis, and thus reducing the Treg/Th17 ratio may slow tumor metastasis (Fig. 2).

Exosomes from M2 macrophages induce the Treg/Th17 imbalance

Due to the high proportion of TAMs in EOC tissues, we examined the relationship between TAMs and T cells. We induced human monocytes into two types of macrophages, M1 (M-CSF$^+$ LPS$^+$IFN-r) and M2 (M-CSF$^+$ IL4), and we used untreated monocytes as a control (Supplementary Fig. S2A–C; ref. 20). Fresh human PB CD14$^+$ monocytes and CD4$^+$ T cells were isolated. The purity of CD4$^+$and CD14$^+$ cells reached 90% (Supplementary Fig. S2D–S2E). After coculturing M1s, M2s, and monocytes with T cells for 3 days, the Treg/Th17 ratio in the M2 group (1.44 ± 0.19) was significantly higher than that in the other two groups ($P = 0.002$, Mann–Whitney test, control: 0.46 ± 0.05; $P < 0.001$, Mann–Whitney test M1: 0.28 ± 0.05; Fig. 3A and B). This result indicated that TAMs might induce an imbalance in the Treg/Th17 ratio in EOC.

Next, we collected the supernatants of monocytes and M1 and M2 macrophages to purify the released exosomes. We used electron microscopy to confirm the sizes of the exosomes and detected exosome biomarkers, including the tetraspanin molecule CD9, CD63, CD81, and Tsg 101 molecules (Fig. 3C and D). We also examined whether exosomes released from macrophages could be taken up by T cells. Labeled exosomes were cocultured with T cells. After 24 hours, T cells were collected and observed by using confocal microscopy. The RNAs in exosomes (green) and exosome membranes (red) were observed in cocultured T cells (Fig. 3E).

Next, we used exosomes from monocytes and M1 and M2 macrophages to coculture with CD4$^+$ T cells. After 3 days, the Treg/Th17 ratio in the M2 group (1.21 ± 0.06) was significantly higher than that in the other two groups ($P = 0.037$, LSD, control: 0.45 ± 0.02; $P = 0.05$, LSD, M1: 0.28 ± 0.07; Fig. 3F). These results indicated that exosomes released from TAMs induced an imbalance in Treg/Th17 cells. The absolute counts and Treg/Th17 ratio in each experiment were also shown as Supplementary Tables S2–S3.

Exosomal miRNAs induce imbalance of Tregs/Th17 cells by targeting STAT3

Exosomes contain miRNAs that can mediate intercellular communication (20, 28). Therefore, we used an Agilent miRNA microarray to profile miRNAs in exosomes released by THP-1 and M2 macrophages (induced from THP-1 cells). Compared with miRNAs in monocyte-secreted exosomes, 42 miRNAs were upregulated and 10 miRNAs were downregulated in M2 macrophage-secreted exosomes (Fig. 4A). Among these, five upregulated miRNAs and one downregulated miRNA were related to T-cell differentiation (Fig. 4B). Thus, we collected the exosomes secreted by primary monocytes and M2 macrophages (induced from primary monocytes), and we found that hsa-miR-21-5p was upregulated 87.79 ± 9.0-fold ($P = 0.001$), hsa-miR-24-3p increased 16.54 ± 0.64-fold ($P = 0.0037$), hsa-miR-29a-3p was upregulated 13.89 ± 1.24-fold ($P = 0.037$), hsa-miR-146b-5p was upregulated 38.9 ± 0.81-fold ($P = 0.037$), and hsa-miR-660-5p was upregulated 14.91 ± 6.60-fold ($P = 0.032$) in exosomes secreted by primary human TAMs compared with monocytes (Fig. 4C).

The miRNA mimics were transfected into CD4$^+$ T cells to determine whether the balance in the CD4$^+$ T-cell subsets changed after transfection. We found that after transferring hsa-miR-29a-3p and hsa-miR-21-5p, the Treg/Th17 ratio increased to a much greater extent than that induced by other miRNAs (Fig. 4D; Supplementary Table S4). This result indicated that hsa-miR-29a-3p and hsa-miR-21-5p in exosomes could alter the ratio of Treg to Th17 cells.

Analysis of the potential targets of these two miRNAs revealed that they could bind to the STAT3 3′UTR (Supplementary Fig. S3A and S3B). Considering that STAT3 is involved in CD4$^+$ T-cell differentiation into Treg or Th17 cells, we analyzed the ability of hsa-miR-29a-3p and hsa-miR-21-5p to regulate STAT3. Western blots showed that STAT3 protein was downregulated in both the CD4$^+$ T-cell parental population (Supplementary Fig. S4A), and in Tregs and Th17 cell subsets after transfection with hsa-miR-29a-3p or hsa-miR-21-5p mimics. The effect was more pronounced after transfection of CD4$^+$ T cells with both mimics together (Fig. 4E). ImageJ analyzed the gray value of protein bands from different groups in Tregs and Th17 cells (Fig. 4F). Real-time PCR analysis revealed reduced STAT3 mRNA expression had a similar trend to protein in the CD4$^+$ T cell parent population and the two subsets (Fig. 4G; Supplementary Fig. S4B). A luciferase assay revealed binding of hsa-miR-29a-3p and hsa-miR-21-5p to the STAT3 3′UTR (Fig. 4H and I).

We were also interested in the downstream effects after hsa-miR-29a-3p and hsa-miR-21-5p combined with STAT3 in T cells. We used RT-PCR to examine expression of IL4, IL6, and TNFα, and IL10 in native CD4$^+$ T cells. Forty-eight hours after transfection, we found that the anti-inflammatory cytokine IL4 was reduced in the hsa-miR-21-5p mimic, hsa-miR-29a-3p mimic transfection group. The group transfected with both mimics had lower values than the NC, whereas the group transfected with both inhibitors showed a higher relative expression. A similar trend was observed for IL6 and TNFα expression, whereas an opposite effect was observed for IL10 expression (Supplementary Fig. S4C–F).

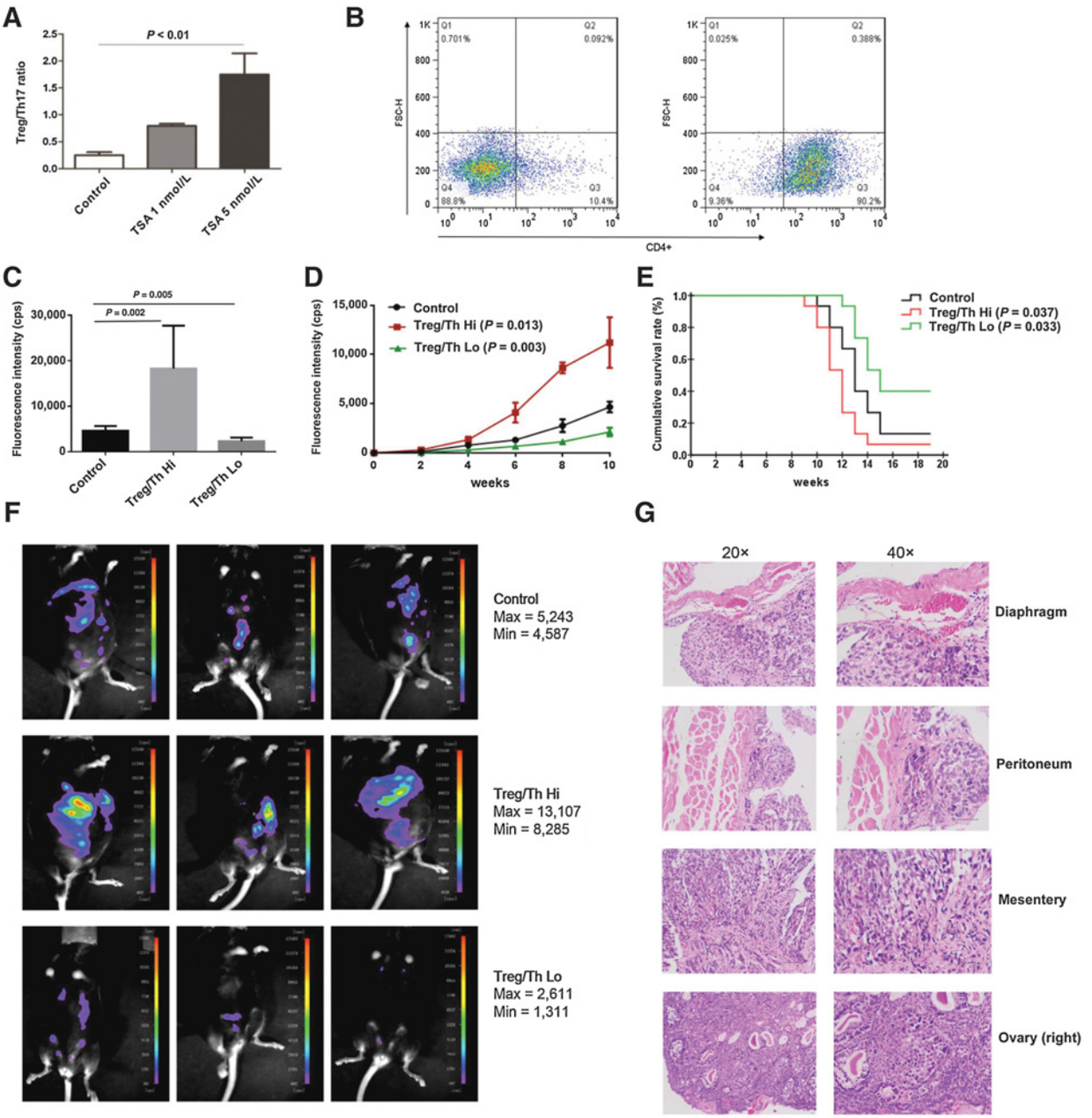

Figure 2.

Effect of the Treg/Th17 imbalance on ovarian cancer *in vivo*. **A,** Trichostatin A (TSA, 5 nmol/L) was used to induce an imbalance in Treg/Th17. Results were from three independent experiments; *t* test. **B,** The purity of $CD4^+$ cells was nearly 90%, as detected by flow cytometry. Image shown on the left is the negative control. Results were from three independent experiments. **C,** At 6 weeks of age, C57BL/6 mice were intraperitoneally injected with ID8-Luc-pur cells (day 1). For the long-term experiments, additional $CD4^+$ T cells were injected beginning (day 15). Each group received 0.1 mL of PBS containing 1×10^6 T cells by i.p. injection once a week. The Treg/Th17-low ratio group was prestimulated with 10 μg/mL anti-CD3 and 5 μg/mL anti-CD28. The Treg/Th17-high ratio group was cultured with 5 nmol/L/mL TSA for an additional 3 days. A bioluminescence imaging system was used to observe the tumor flux (cps) on day 2 and the following weeks. Days 1 to 8 were recorded as the first week. The tumor fluorescence intensity (cps) was analyzed in the three groups after injection of ID8-Luc-pur cells at 11 weeks ($n = 15$ mice/per group); *t* test**. D,** Fluorescence intensity (cps) in the three groups after injection of ID8-Luc-pur cells at 2–10 weeks (every 2 weeks); $n = 15$ mice/per group; *t* test. **E,** Kaplan–Meier curve showing the cumulative survival rate of the three groups ($n = 15$ mice/group); log-rank test. **F,** Typical images of the three groups at week 11. **G,** Hematoxylin–eosin (H&E) staining of the peritoneum, mesentery, and diaphragm tissue from sacrificed mice. $P < 0.05$ was considered statistically significant.

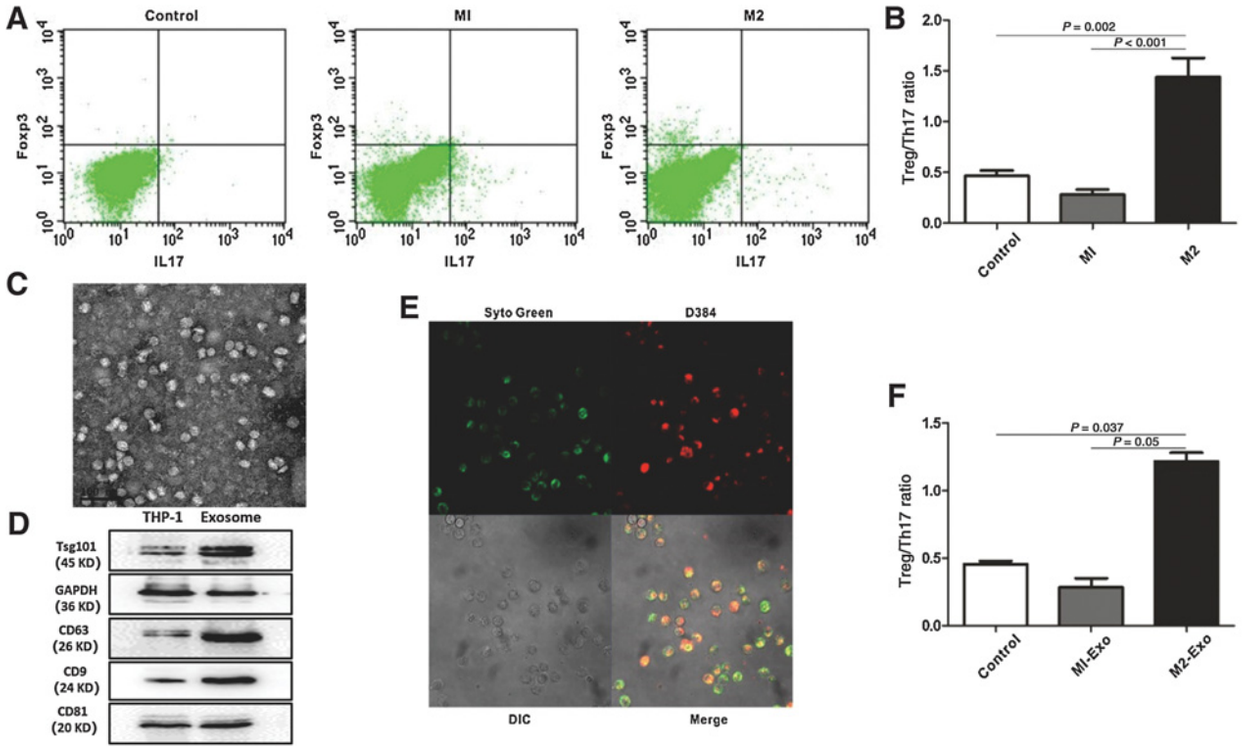

Figure 3.

M2 macrophages induce an imbalance in Tregs and Th17 cells via exosome delivery. **A,** $CD4^+$ T cells were cocultured with control, M1, or M2 macrophages for 3 days, and the proportion of Th17 cells and Tregs was detected by flow-cytometric analysis. Results were from 10 independent experiments**. B,** The Treg/Th17 ratio in the three groups, $n = 10$/group; *t* test. **C,** Transmission electron microscopy image of exosomes collected from the supernatants of M2 macrophages. Results were from three independent experiments. Scale bar, 100 nm. **D,** Western blot analysis of CD9, CD 63, CD81, and Tsg 101 in exosomes using THP-1 cells as a control. Results were from three independent experiments. **E,** Exosomes secreted by M2 macrophages were labeled using SYTO RNASelect Green Fluorescent Cell Stain (RNA was shown as bright green fluorescence) and a red fluorescent membrane stain and cocultured with T cells for 24 hours. The T cells were collected for confocal microscopy to detect M2 macrophage–derived exosomes in T cells. RNA in exosomes (top left), exosome membranes (top right), T cells under a light microscope (bottom left), and merged image (bottom right). Results were from two independent experiments. **F,** T cells were cocultured with control or with exosomes from M1 or M2 macrophages for 3 days. The proportions of Th17 and Tregs were determined by flow-cytometric analysis, and the Treg/Th17 ratio was calculated, $n = 3$/group; *t* test. $P < 0.05$ was considered statistically significant.

We used flow-cytometric analysis to detect cytokines from the two T-cell subsets, including TGFβ, IL10, and IL4 for Tregs and TNFα and IL6 for Th17 cells. First, we confirmed that the purity of Tregs and Th17 cells reached 85% (Supplementary Fig. S5A–S5B). We found that IL4 in Tregs was reduced in the hsa-miR-21-5p mimic and hsa-miR-29a-3p mimic transfection groups ($P = 0.008$, $P = 0.016$, *t* test), and the group transfected with both mimics had lower values than the NC group ($P = 0.001$, *t* test). The group transfected with both inhibitors showed a higher relative expression ($P = 0.035$, *t* test). A similar trend was observed for TNFα and IL6 in Th17 cells. However, opposite effects were observed for TGFβ and IL10 in Tregs (Fig. 4J and K). These results showed that after transfection, native $CD4^+$ T cells with hsa-miR-29a-3p, hsa-miR-21-5p, the cytokines IL4, IL6, and TNFα were downregulated and the anti-inflammatory cytokines TGFβ and IL10 were upregulated (Supplementary Fig. S5C–S5G; Supplementary Table S5). These results indicated that the combined effect of the two mimics was more pronounced than that of either mimic alone. These factors together might be responsible for the imbalance in the EOC immune microenvironment, ultimately leading to tumor progression.

Effect of mmu-miR-29a-3p and mmu-miR-21-5p on ovarian cancer metastasis.

To explore the effect of mmu-miR-29a-3p and mmu-miR-21-5p on the metastasis of ovarian cancer *in vivo*, we established a metastasizing ovarian cancer C57BL/6 model as previously described. The five groups were named according to the different T-cell treatments. T cells were transfected with NC, mmu-miR-21-5p mimic, mmu-miR-29a-3p mimic, both mimics, or both inhibitors. Before *in vivo* experiments, mouse transfected $CD4^+$ T cells had the Treg/Th17 ratio measured after 72 hours (Supplementary Fig. S6A–S6E). The trend is consistent with *in vitro* experiments, we found that the Treg/Th17 ratio was increased in the mmu-miR-21-5p mimic and mmu-miR-29a-3p mimic groups. The group transfected with both mimics had higher Treg/Th17 ratio than NC, whereas the group transfected with both inhibitors showed a lower Treg/Th17 ratio (Supplementary Fig. S6F). For every experiment, we detected the transfection efficiency with a fluorescence microscope 6 hours after transfection (Supplementary Fig. S7A).

In the *in vitro* experiment, the relative STAT3 expression (fold change) in the five groups was examined using real-time PCR after 48 hours of transfection in three independent experiments. The

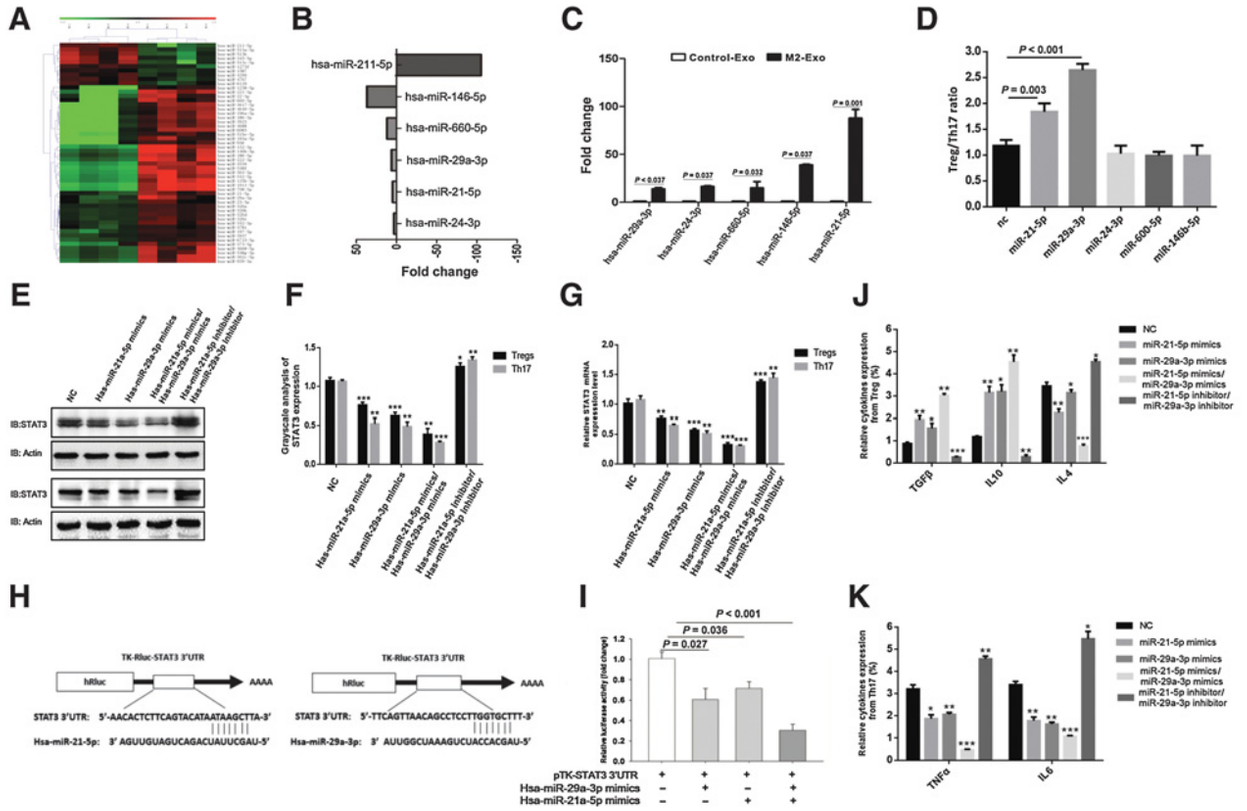

Figure 4.

Hsa-miR-29a-3p and hsa-miR-21-5p from TAM-secreted exosomes induce a Treg/Th17 imbalance and alters cytokines by targeting STAT3. **A,** Heat map of miRNAs expressed in THP-1 cells and THP-1–induced M2 macrophages. **B,** MiRNAs related to T-cell differentiation. **C,** The expression of five upregulated miRNAs in primary monocytes and M2 macrophages. Three duplicate wells/per group. Results were from three independent experiments; *t* test**. D,** Hsa-miR-21-5p and hsa-miR-29a-3p mimics were transfected to $CD4^+$ T cells for 3 days. The proportion of Th17 and Tregs was detected by flow cytometry. The Treg/Th17 ratio was calculated. Results were from three independent experiments; *t* test**. E,** Western blot analysis was used to detect STAT3 protein in Tregs (the top images) and Th17 cells (the bottom images) after $CD4^+$ T cells were transfected with NC, hsa-miR-21-5p mimic, hsa-miR-29a-3p mimic, both mimics, or both inhibitors. Results were from three independent experiments. **F,** ImageJ analyzed gray value of protein bands from different groups in Tregs and Th17 cells. $n = 3$/group, *t* test. *, $P < 0.05$; **, $P < 0.01$; ***, $P < 0.001$. **G,** RT-PCR was used to detect the STAT3 mRNA in Tregs and Th17 cells after native $CD4^+$ T cells were transfected with NC, hsa-miR-21-5p mimic, hsa-miR-29a-3p mimic, both mimics, or both inhibitors. Three duplicate wells/per group. Results were from three independent experiments; *t* test. *, $P < 0.05$; **, $P < 0.01$; ***, $P < 0.001$. **H,** Prediction of the binding site of hsa-miR-21-5p and hsa-miR-29a-3p in the STAT3 gene sequence by the target scan. **I,** Luciferase assay revealing binding of hsa-miR-29a-3p and hsa-miR-21 to the STAT3 3′UTR. $n = 3$/group; *t* test. **J** and **K,** Expression of cytokines TGFβ, IL10, IL4 in Tregs, and TNFα or IL6 in Th17 cells after native $CD4^+$ T cells were transfected with NC, hsa-miR-21-5p mimic, hsa-miR-29a-3p mimic, both mimics, or both inhibitors. Results were from three independent experiments; *t* test. *, $P < 0.05$; **, $P < 0.01$; ***, $P < 0.001$.

mmu-miR-21-5p mimic, mmu-miR-29a-3p mimic, both mimics, and both inhibitors groups showed a significant difference compared with the NC group. The expression of STAT3 was decreased in the mmu-miR-21-5p mimic and mmu-miR-29a-3p mimic groups. The group transfected with both mimics had lower STAT3 expression than NC, whereas the group transfected with both inhibitors showed a higher STAT3 expression (Fig. 5A, *t* test). We did not set up a mmu-miR-21-5p inhibitor or mmu-miR-29a-3p inhibitor group because the individual inhibitors did not have a significant effect on improving STAT3 expression *in vitro* (Supplementary Fig. S7B–S7C). STAT3 was detected by Western blotting after 72 hours of transfection (Fig. 5B). The proportion of Tregs and Th17 cells was tested at the same time after 72 hours of transfection.

After injecting ID8-Luc-pur cells, we used the bioluminescence imaging system to observe tumor growth. The mmu-miR-21-5p mimic (tumor flux 4882.60 ± 99.14 cps, $P = 0.001$, *t* test) and the mmu-miR-29a-3p mimic group (tumor flux 4647.80 ± 236.99 cps, $P = 0.002$, *t* test) showed an enhancement in tumor load on week 10 compared with the NC group (3011.40 ± 75.98 cps), and the group with both mimics (tumor flux 8704.00 ± 672.42 cps, $P = 0.001$, unpaired *t* test) showed even stronger flux, whereas the group with both inhibitors (tumor flux 2150.60 ± 97.25 cps, $P = 0.001$, *t* test) showed weak flux (Fig. 5C). Tumor load for the mmu-miR-21-5p mimic group, the mmu-miR-29a-3p mimic group, both mimics group increased more rapidly than that of the control group ($P = 0.001$, $P = 0.002$, $P < 0.001$, respectively, *t* test), and the group with both inhibitors exhibited slower tumor growth than that of the control ($P = 0.008$, $n = 5$, *t* test; Fig. 5D). This result was also consistent with the cumulative survival rate changes over time. The group with both inhibitors had a longer median survival time than the control group ($P = 0.034$, log-rank

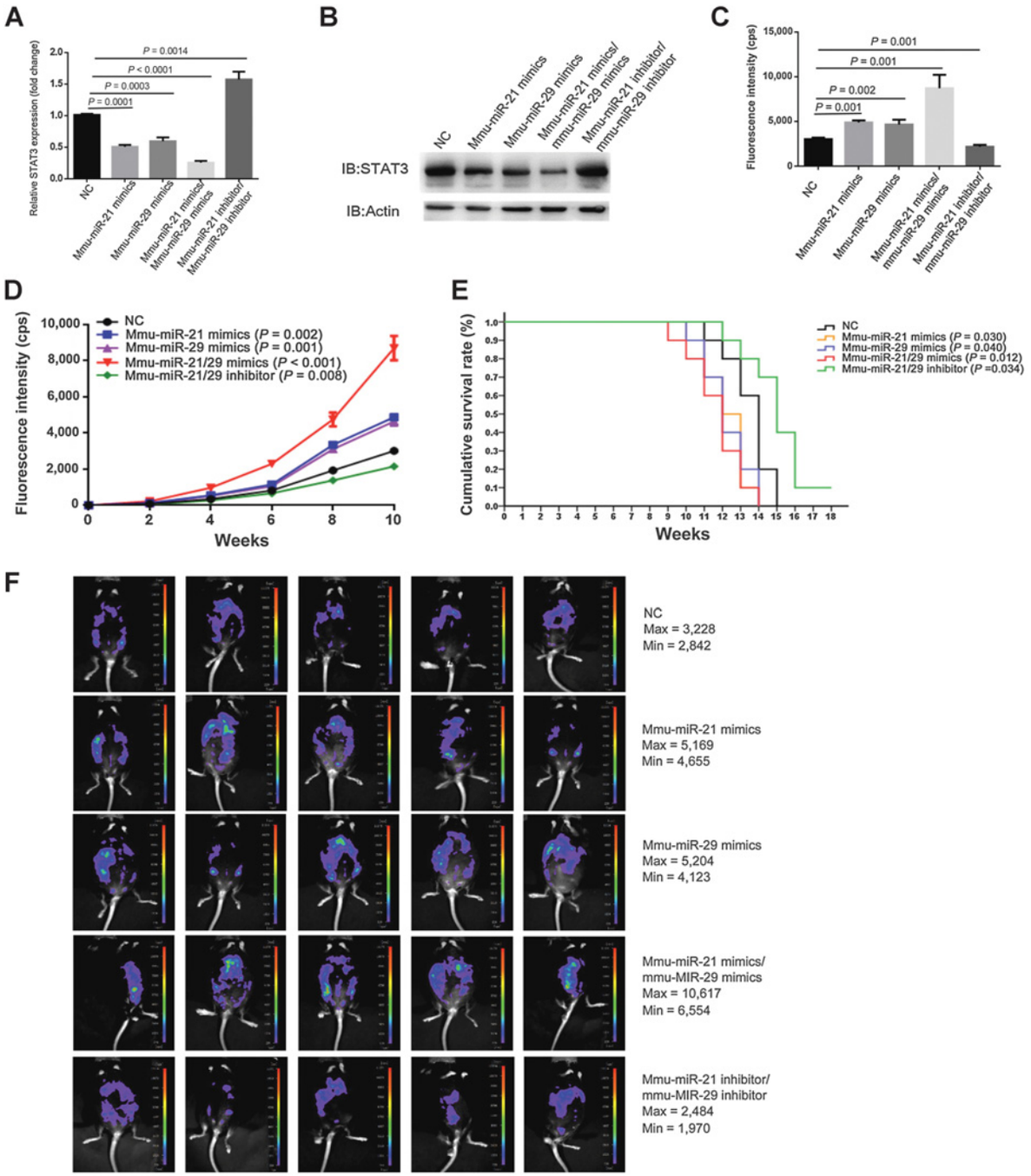

Figure 5.

Effect of mmu-miR-29a-3p and mmu-miR-21 on the growth and metastasis of ovarian cancer *in vivo*. **A,** For T cells that received NC, mmu-miR-21-5p mimic, mmu-miR-29a-3p mimic, both mimics, or both inhibitors after 48 hours, the relative STAT3 expression (fold change) in the five groups was examined using real-time PCR; three duplicate wells/per group. Results were from three independent experiments; *t* test**. B,** After the T cells were transfected with NC, mmu-miR-21-5p mimic, mmu-miR-29a-3p mimic, both mimics, or both inhibitors for 72 hours, STAT3 was detected via Western blotting in three independent experiments. **C,** The tumor fluorescence intensity (cps) in the five groups after injection of ID8-Luc-pur cells for 10 weeks; $n = 10$ mice/per group, *t* test. **D,** At 6 weeks of age, C57BL/6 mice were intraperitoneally injected with ID8-Luc-pur cells (day 1). For long-term experiments, additional T-cell injections were initiated (day 15). Each group received 0.1 mL of PBS containing 1×10^6 $CD4^+$ T cells via i.p. injection once a week. The T cells were transfected with NC, mmu-miR-21-5p mimic, mmu-miR-29a-3p mimic, both mimics, or both inhibitors for 72 hours. A bioluminescence imaging system was used to observe tumor flux (cps) on day 2 and each following week. Days 1 to 8 were recorded as the first week. Tumor fluorescence intensity (cps) in the 5 groups after injecting ID8-Luc-pur cells for 2 to 10 weeks (every 2 weeks); $n = 10$ mice/per group, *t* test. **E,** Kaplan–Meier curve showing the cumulative survival rate of the five groups; $n = 10$ mice/per group; log-rank test. **F**, Typical images of mice in the five groups are presented for week 10. $P < 0.05$ was considered statistically significant.

test), and the group with both mimics was shortest ($P = 0.012$, log-rank test; Fig. 5E). The tumor flux (cps) was recorded in the three groups every week, and typical images are presented (week 10; Fig. 5F). We harvested the peritoneum, mesentery, and diaphragm from mice, and these tissues showed tumor metastases. The peritoneum was cut to a similar size for comparison among groups (Supplementary Fig. S7D). After observing and recording the time to tumor formation and metastasis via live imaging, we detected the effect of mmu-miR-29a-3p and mmu-miR-21-5p on ovarian cancer *in vivo*. We concluded that mmu-miR-29a-3p and mmu-miR-21-5p could bind STAT3 in T cells and induce an imbalance in the Treg/Th17 cell ratio, which then enhanced the growth and metastasis of tumor cells *in vivo* (Fig. 5).

The Treg/Th17 imbalance is associated with EOC grade and patient survival.

The association between the Treg/Th17 ratio and clinicopathologic variables in EOC patients is shown in Table 1 and Supplementary Table S1. We also compared the sensitivity and specificity of the Treg/Th17 ratio in EOC patients (Fig. 6A). Based on the ROC curve, an applicable Treg/Th17 ratio of 1.02 yielded the best predictive value for OS. When the applicable Treg/Th17 ratio cutoff value was used, the EOC patients with a Treg/Th17 ratio greater than 1.02 exhibited a significantly shorter OS (40.16 ± 1.94 months) than those with a Treg/Th17 ratio less than 1.02 (51.00 ± 4.87 months, $P = 0.043$; Fig. 6B).

We also analyzed the relationship between the Treg/Th17 ratio and EOC patients in the TCGA database. A heat map depicted the relative abundances of related cells or molecules among the 467 patients (Supplementary Fig. S8A). The Treg/Th17 ratio was associated with histologic grade and was an independent prognostic factor for OS of EOC patients ($P = 0.0369$, Mantel–Haenszel test; Fig. 6C). Simultaneous high expression of both miR-29a-3p and miR-21-5p was associated with poor OS ($P = 0.0459$, Mantel–Haenszel test; Fig. 6D). However, no significant difference between survival rates and M1/M2 proportion or IL4, IL6, IL10, and TNFα expression was found (Supplementary Fig. S8B-G). Taken together, we propose that exosomes released from TAMs transfer hsa-miR-29a-3p and hsa-miR-21-5p to $CD4^+$ T cells. A Treg/Th17 imbalance is then induced via STAT3 interaction, leading to tumor progression in EOC (Fig. 6E).

Discussion

Research indicates that cancer is a system that includes both cancer cells and the TME, which includes TAMs and T lymphocytes. Tregs and Th17 cells, two subtypes of $CD4^+$ T cells, play opposite roles in immune regulation, even though they share a common differentiation pathway. It has been verified that $IL17^+$ T-cell differentiation is accompanied by enhanced Treg accumulation both *in vitro* and *in vivo* (29). Others have found that the Th17/Treg ratio and related cytokines are also significantly higher in patients with non–small cell lung cancer (NSCLC) and that the Th17/Treg ratio positively correlates with the carcinoembryonic antigen concentrations in NSCLC patients (30). The Treg/Th17 imbalance has also been observed in colon cancer, bladder carcinoma, and breast cancer (17–19). IL17A, IL23, IL10, and TGFβ1 expression significantly changes after the Treg/Th17 imbalance (31). Given the competition between these two cell types, studying the imbalance between T-cell subsets in the TME might help understand tumor progression. In addition to Treg and Th17 cell subsets, the TME includes a complex network of immune T-cell subsets such as Th1 and Th2 cells. Th1 cells had effects opposite to those of Th17 cells on patient survival in colorectal cancer (32), perhaps because of associated increased expression of CX3CL1 and memory T-cell responses (33). However, other T-cell subsets may not mediate direct tumor cytotoxic activity.

In this study, we found that the Treg/Th17 ratio was significantly higher in ovarian cancer tissues and peritoneal tissues than in benign patient tissues. The Treg/Th17 ratio was higher in SOC than in NSOC, suggesting that the imbalance in T-cell subsets might be associated with worse outcomes. The relationship between Treg/Th17 ratio and EOC patients among 467 patients' OS was evaluated in the TCGA database. The Treg/Th17 ratio was associated with histologic grade and was an independent prognostic factor for OS of EOC patients. We confirmed *in vivo* that a high Treg/Th17 ratio facilitated tumor progression and metastasis into the peritoneum. Thus, the Treg/Th17 imbalance promotes EOC progression both *in vivo* and *in vitro*.

The upstream mechanisms of the Treg/Th17 imbalance in tumor progression require further research. The interactions between cells in the TME may be one of the underlying factors inducing the Treg/Th17 imbalance. As the most abundant immune cells in EOC, TAMs have many roles in regulating the function of T cells. TAMs can recruit Tregs and promote colorectal cancer development in mice (34). Our previous study also showed that Tie2-expressing monocytes, a subtype TAMs, modulates angiogenesis and metastasis of EOC via cross-talk between endothelial cells (35). The current results showed that M2 macrophages skewed the Treg/Th17 balance when cocultured with T cells due to release of exosomes into the supernatant. Few studies have examined the mechanism by which TAMs induce Treg and Th17 differentiation and polarization. Our study provides further insights into the upstream mechanisms of the Treg/Th17 imbalance.

Exosomes derived from multivesicular endosomes can shuttle miRNAs into adjacent target cells and regulate cellular functions within the microenvironment (36). To further illustrate the factors involved in TAM exosome-mediated T-cell differentiation, we explored the miRNAs in exosomes from the M0 and M2 macrophages via microarray analysis. We chose 5 miRNAs to study: hsa-miR-21-5p, hsa-miR-24-3p, hsa-miR-29a-3p, hsa-miR-146b-5p, and hsa-miR-660-5p, reported to have a possible role in T-cell differentiation (37). Further functional studies revealed that hsa-miR-29a-3p and hsa-miR-21-5p were the key miRNAs in exosomes that regulate T-cell differentiation and polarization both *in vivo* and *in vitro*. Simultaneous high expression of miR-29a-3p and miR-21-5p was associated with poor OS in the TCGA database. The miR-29 family belongs to the list of key miRNAs in the adaptive immune system (38). MiR-21, a tumor onco-miRNA, is frequently overexpressed in various tumors, including pancreatic cancer and EOC (39).

Our molecular mechanism studies showed that hsa-miR-29a-3p and hsa-miR-21-5p directly targeted STAT3 in $CD4^+$ T cells. It has been reported that various miRNAs can regulate STAT3 to affect downstream mechanisms. For example, miR-124 regulates T cell–mediated immunosuppression in glioma by targeting STAT3 (40). Hsa-miR-29a has been reported to target STAT3 in monocytes during sepsis (41), and miR-21 can target STAT3 in breast cancer (42). STAT3 plays a critical role in Treg and Th17 cell differentiation (43). One reported mechanism is that STAT3

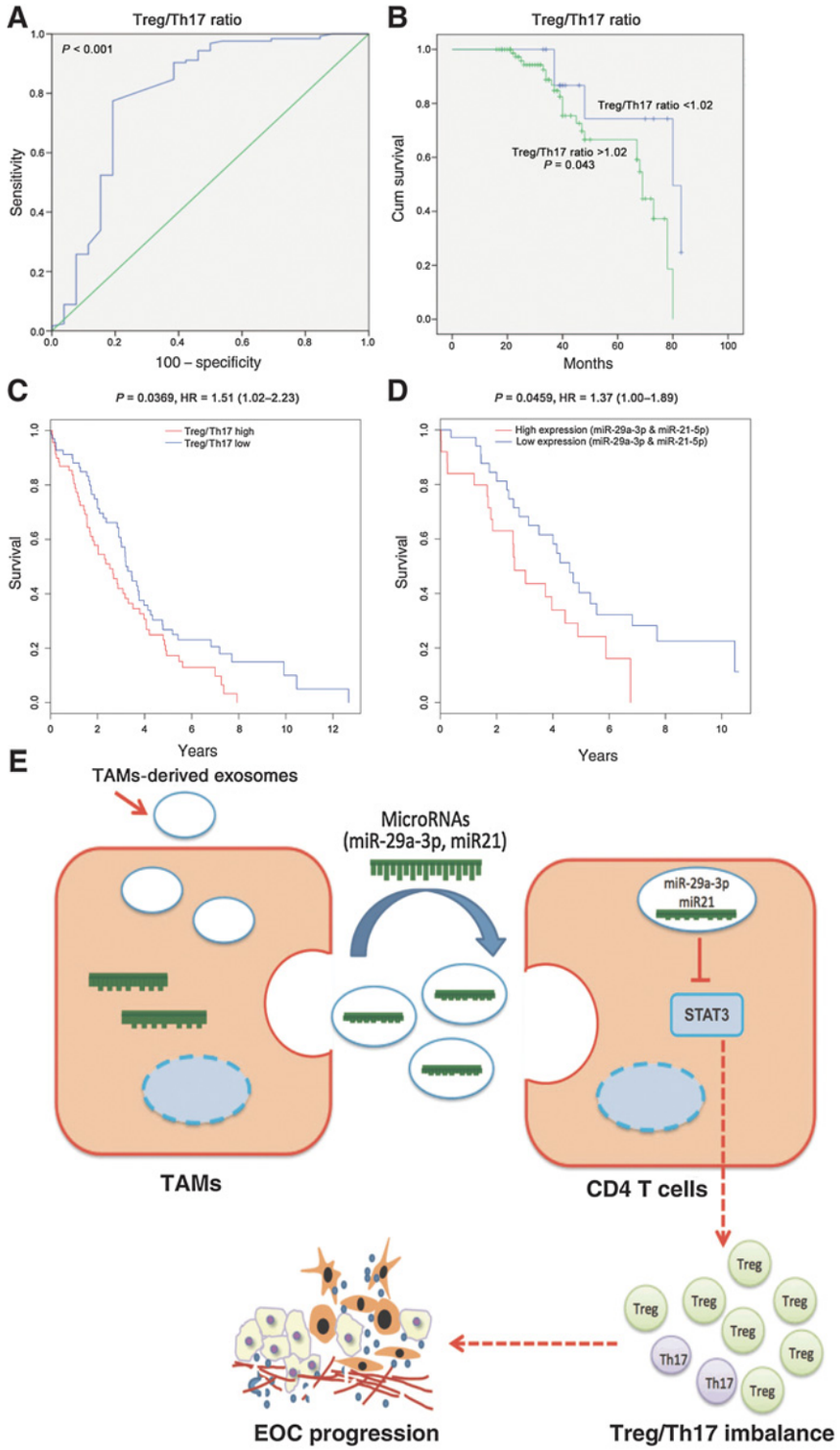

Figure 6.

The imbalance in Treg/Th17 cells was associated with EOC grade and patient survival. **A,** The ROC curve reflecting the sensitivity and specificity of the Treg/Th17 ratio in EOC patients. **B,** EOC patient survival based on the Treg/Th17 ratio cutoff of 1.02. **C,** The relationship between Treg/Th17 ratio and OS among 467 EOC patients in the TCGA database. **D,** The relationship between miR-29a-3p and miR-21-5p expression and OS among 467 EOC patients in the TCGA database. **E,** Illustration of our conclusions. TAM-derived exosomes transfer miR-29a-3p and miR-21-5p to synergistically induce a Treg/Th17 cell imbalance through directly targeting of STAT3 in $CD4^+$ T cells.

binds to intron1 of the RORc gene and activates Sox5t to stimulate RORc, thus inducing Th17 cell differentiation (44). Our results indicated that STAT3 may regulate the Treg/Th17 balance in the EOC microenvironment. Inhibition of STAT3 signaling has revealed that it is a crucial pathway in the reciprocal regulation of Th17 and Tregs (43, 45). We also found that hsa-miR-29a-3p and hsa-miR-21-5p targeted STAT3 synergistically in $CD4^+$ T cells. Our study reveals a function of miR-21-5p in tumor biology,

specifically targeting STAT3 in $CD4^+$ T cells in TME, and thus provides further evidence supporting miR-21-5p as a tumor onco-miRNA.

As a member of the mammalian Janus kinase (Jak) family, STAT3 mediates inflammatory immune responses by converting cytokine signals into immune cell differentiation (46). Interactions between cytokines and STAT3 have also been widely reported. For example, STAT3-deficient follicular T helper cells overexpress both IL4 and Bcl6 (47). IL22 and IL17 production has to be controlled tightly and independently, and STAT3 and retinoid orphan receptor γt (RORγt) drive the expression of both IL22 and IL17 (48). Our study showed that after miR-29a-3p and miR-21-5p bind with STAT3 in $CD4^+$T cells, the cytokines IL4, IL6, and TNFα were downregulated and the anti-inflammatory cytokine IL10 was upregulated. Generally, proinflammatory and anti-inflammatory cytokine changes were responsible for the imbalance of immune microenvironment, ultimately leading to tumor progression. Th17-produced cytokines, such as IL6 and TNFα, synergistically activate NF-kB to promote colorectal cancer cell growth (23). IL4 and IL13 are anti-inflammatory, immunoregulatory cytokines that can influence cancer-directed immunosurveillance (49). In contrast, IL10 has been shown to enhance the effector function of activated human $CD8^+$ T cells by increasing cytolytic activity (50). In conclusion, our study found that TAM-derived exosomes transferred miRNAs targeting STAT3 to T cells and regulated T-cell subset polarization, resulting in a Treg/Th17 imbalance that promoted tumor progression. Targeting exosomes or these miRNAs might represent an approach for treating cancer.

Disclosure of Potential Conflicts of Interest

No potential conflicts of interest were disclosed.

Authors' Contributions

Conception and design: J. Zhou, X. Wu, T. Zhang, H. Wang, K. Wang, Y. Lin, X. Wang

Development of methodology: X. Wu, Y. Lin, X. Wang

Acquisition of data (provided animals, acquired and managed patients, provided facilities, etc.): J. Zhou, X. Wu, Q. Zhu, X. Wang, H. Wang, X. Wang

Analysis and interpretation of data (e.g., statistical analysis, biostatistics, computational analysis): X. Li, X. Wu, Y. Lin

Writing, review, and/or revision of the manuscript: X. Li, Q. Zhu, X. Wang, Y. Lin

Administrative, technical, or material support (i.e., reporting or organizing data, constructing databases): J. Zhou, X. Wu, Y. Lin, X. Wang

Study supervision: Y. Lin, X. Wang

Acknowledgments

This study was supported by grants from the National Natural Science Foundation of China (81372787, 81402042, 81602280, and 81874103), Shanghai Hospital Development Center Action Plan (16CR4028A), and the Science and Technology Commission of Shanghai Municipality (STCSM, 17411968100).

The authors thank Shanghai First Maternity and Infant Hospital for providing patients specimens to facilitate clinical information analysis.

The costs of publication of this article were defrayed in part by the payment of page charges. This article must therefore be hereby marked *advertisement* in accordance with 18 U.S.C. Section 1734 solely to indicate this fact.

Received August 31, 2017; revised February 22, 2018; accepted October 29, 2018; published first November 5, 2018.

References

1. Siegel RL, Miller KD, Jemal A. Cancer statistics, 2016. CA Cancer J Clin 2016;66:7–30.
2. Sceneay J, Smyth MJ, Moller A. The pre-metastatic niche: finding common ground. Cancer Metastasis Rev 2013;32:449–64.
3. Wang X, Deavers M, Patenia R, Bassett RL Jr, Mueller P, Ma Q, et al. Monocyte/macrophage and T-cell infiltrates in peritoneum of patients with ovarian cancer or benign pelvic disease. J Transl Med 2006;4:30.
4. Zhu Q, Wu X, Wu Y, Wang X. Interaction between Treg cells and tumor-associated macrophages in the tumor microenvironment of epithelial ovarian cancer. Oncol Rep 2016;36.
5. Kumar V, Cheng P, Condamine T, Mony S, Languino LR, McCaffrey JC, et al. CD45 Phosphatase Inhibits STAT3 transcription factor activity in myeloid cells and promotes tumor-associated macrophage differentiation. Immunity 2016;44:303–15.
6. Zhang M, He Y, Sun X, Li Q, Wang W, Zhao A, et al. A high M1/M2 ratio of tumor-associated macrophages is associated with extended survival in ovarian cancer patients. J Ovarian Res 2014;7:19.
7. Binnemarspostma K, Storm G, Prakash J. Nanomedicine strategies to target tumor-associated macrophages. Int J Mol Sci 2017;18:979.
8. Brown JM, Recht L, Strober S. The promise of targeting macrophages in cancer therapy. Clin Cancer Res 2017;23:clincanres.3122.2016.
9. Liu Y, Zhao L, Li D, Yin Y, Zhang CY, Li J, et al. Microvesicle-delivery miR-150 promotes tumorigenesis by up-regulating VEGF, and the neutralization of miR-150 attenuate tumor development. Protein Cell 2013;4:932–41.
10. Zhu Y, Chen X, Pan Q, Wang Y, Su S, Jiang C, et al. A comprehensive proteomics analysis reveals a secretory path- and status-dependent signature of exosomes released from tumor-associated macrophages. J Proteome Res 2015;14:4319–31.
11. Record M, Carayon K, Poirot M, Silvente-Poirot S. Exosomes as new vesicular lipid transporters involved in cell-cell communication and various pathophysiologies. Biochim Biophys Acta 2014;1841:108–20.
12. EL Andaloussi S, Mäger I, Breakefield XO, Wood MJ. Extracellular vesicles: biology and emerging therapeutic opportunities. Nat Rev Drug Discov 2013;12:347–57.
13. Li X, Wang X. The emerging roles and therapeutic potential of exosomes in epithelial ovarian cancer. Mol Cancer 2017;16:92.
14. Hunder NN, Wallen H, Cao J, Hendricks DW, Reilly JZ, Rodmyre R, et al. Treatment of metastatic melanoma with autologous CD4+ T cells against NY-ESO-1. N Engl J Med 2008;358:2698–703.
15. Charbonneau B, Moysich KB, Kalli KR, Oberg AL, Vierkant RA, Fogarty ZC, et al. Large-scale evaluation of common variation in regulatory T cell-related genes and ovarian cancer outcome. Cancer Immunol Res 2014;2:332–40.
16. Maruyama T, Kono K, Mizukami Y, Kawaguchi Y, Mimura K, Watanabe M, et al. Distribution of Th17 cells and FoxP3(+) regulatory T cells in tumor-infiltrating lymphocytes, tumor-draining lymph nodes and peripheral blood lymphocytes in patients with gastric cancer. Cancer Sci 2010;101:1947–54.
17. Duan MC, Zhong XN, Liu GN, Wei JR. The Treg/Th17 paradigm in lung cancer. J Immunol Res 2014;2014:730380.
18. Mougiakakos D, Choudhury A, Lladser A, Kiessling R, Johansson CC. Regulatory T cells in cancer. Adv Cancer Res 2010;107:57–117.
19. Chi LJ, Lu HT, Li GL, Wang XM, Su Y, Xu WH, et al. Involvement of T helper type 17 and regulatory T cell activity in tumour immunology of bladder carcinoma. Clin Exp Immunol 2010;161:480–9.
20. Solinas G, Schiarea S, Liguori M, Fabbri M, Pesce S, Zammataro L, et al. Tumor-conditioned macrophages secrete migration-stimulating factor: a new marker for M2-polarization, influencing tumor cell motility. J Immunol 2010;185:642–52.
21. Stewart CA, Metheny H, Iida N, Smith L, Hanson M, Steinhagen F, et al. Interferon-dependent IL-10 production by Tregs limits tumor Th17 inflammation. J Clin Invest 2013;123:4859–74.
22. Grivennikov SI, Greten FR, Karin M. Immunity, inflammation, and cancer. Cell 2010;140:883–99.

23. Simone VD, Franzè E, Ronchetti G, Colantoni A, Fantini MC, Fusco DD, et al. Th17-type cytokines, IL-6 and TNF-α synergistically activate STAT3 and NF-kB to promote colorectal cancer cell growth. Oncogene 2015;34: 3493.
24. Powrie F, Leach MW, Mauze S, Caddle LB, Coffman RL. Phenotypically distinct subsets of CD4+ T cells induce or protect from chronic intestinal inflammation in C. B-17 scid mice. Int Immunol 1993;5:1461–71.
25. Xu S, Tao Z, Hai B, Liang H, Shi Y, Wang T, et al. miR-424(322) reverses chemoresistance via T-cell immune response activation by blocking the PD-L1 immune checkpoint. Nat Commun 2016;7:11406.
26. Cai Q, Yan L, Yan X. Anoikis resistance is a critical feature of highly aggressive ovarian cancer cells. Oncogene 2015;34:3315–24.
27. Li H, Wang D, Zhang H, Kirmani K, Zhao Z, Steinmetz R, et al. Lysophosphatidic acid stimulates cell migration, invasion, and colony formation as well as tumorigenesis/metastasis of mouse ovarian cancer in immunocompetent mice. Mol Cancer Therapeutics 2009;8:1692.
28. Papadopoulou AS, Dooley J, Linterman MA, Pierson W, Ucar O, Kyewski B, et al. The thymic epithelial microRNA network elevates the threshold for infection-associated thymic involution via miR-29a mediated suppression of the IFN-alpha receptor. Nat Immunol 2012;13:181–7.
29. Li S, Li Y, Qu X, Liu X, Liang J. Detection and significance of TregFoxP3(+) and Th17 cells in peripheral blood of non-small cell lung cancer patients. Arch Med Sci 2014;10:232–9.
30. Duan MC, Han W, Jin PW, Wei YP, Wei Q, Zhang LM, et al. Disturbed Th17/Treg balance in patients with non-small cell lung cancer. Inflammation 2015;38:2156–65.
31. Ding JW, Zheng XX, Zhou T, Tong XH, Luo CY, Wang XA. HMGB1Modulates the Treg/Th17 Ratio in Atherosclerotic Patients. J Atherosclerosis Thrombosis 2016;23:737–45.
32. Tosolini M, Kirilovsky A, Mlecnik B, Fredriksen T, Mauger S, Bindea G, et al. Clinical impact of different classes of infiltrating T cytotoxic and helper cells (Th1, th2, treg, th17) in patients with colorectal cancer. Cancer Res 2011;71:1263–71.
33. Mlecnik B, Tosolini M, Charoentong P, Kirilovsky A, Bindea G, Berger A, et al. Biomolecular Network Reconstruction Identifies T-Cell homing factors associated with survival in colorectal cancer. Gastroenterology 2010;138:1429–40.
34. Liu J, Ning Z, Li Q, Zhang W, Fang K, Leng Q, et al. Tumor-associated macrophages recruit CCR6^{+} regulatory T cells and promote the development of colorectal cancer via enhancing CCL20 production in mice. Plos One 2011;6:e19495.
35. Wang X, Zhu Q, Lin Y, Wu L, Wu X, Wang K, et al. Crosstalk between TEMs and endothelial cells modulates angiogenesis and metastasis via IGF1-IGF1R signalling in epithelial ovarian cancer. Br J Cancer 2017;117: 1371–82.
36. Camussi G, Deregibus MC, Bruno S, Cantaluppi V, Biancone L. Exosomes/microvesicles as a mechanism of cell-to-cell communication. Kidney Int 2010;78:838–48.
37. Au Yeung CL, Co NN, Tsuruga T, Yeung TL, Kwan SY, Leung CS, et al. Exosomal transfer of stroma-derived miR21 confers paclitaxel resistance in ovarian cancer cells through targeting APAF1. Nat Commun 2016;7: 11150.
38. Liston A, Linterman M, Lu LF. MicroRNA in the adaptive immune system, in sickness and in health. J Clin Immunol 2010;30:339–46.
39. Takikawa T, Masamune A, Yoshida N, Hamada S, Kogure T, Shimosegawa T. Exosomes derived from pancreatic stellate cells: MicroRNA signature and effects on pancreatic cancer cells. Pancreas 2017;46:19–27.
40. Wei J, Wang F, Kong LY, Xu S, Doucette T, Ferguson SD, et al. miR-124 inhibits STAT3 signaling to enhance T cell-mediated immune clearance of glioma. Cancer Res 2013;73:3913–26.
41. Song X, Wang CT, Geng XH. MicroRNA-29a promotes apoptosis of monocytes by targeting STAT3 during sepsis. Genet Mol Res 2015;14: 13746–53.
42. Zhang C, Liu K, Li T, Fang J, Ding Y, Sun L, et al. miR-21: A gene of dual regulation in breast cancer. Int J Oncol 2016;48:161–72.
43. Zheng Y, Wang Z, Deng L, Zhang G, Yuan X, Huang L, et al. Modulation of STAT3 and STAT5 activity rectifies the imbalance of Th17 and Treg cells in patients with acute coronary syndrome. Clin Immunol 2015;157:65–77.
44. Durant L, Watford WT, Ramos HL, Laurence A, Vahedi G, Wei L, et al. Diverse targets of the transcription factor STAT3 contribute to T cell pathogenicity and homeostasis. Immunity 2010;32:605–15.
45. Chaudhry A, Samstein RM, Treuting P, Liang Y, Pils MC, Heinrich JM, et al. Interleukin-10 signaling in regulatory T cells is required for suppression of Th17 cell-mediated inflammation. Immunity 2011;34:460–2.
46. Saeki Y, Nagashima T, Kimura S, Okada-Hatakeyama M. An ErbB receptor-mediated AP-1 regulatory network is modulated by STAT3 and c-MYC during calcium-dependent keratinocyte differentiation. Exp Dermatol 2012;21:293–8.
47. Wu H, Xu LL, Teuscher P, Liu H, Kaplan MH, Dent AL. An inhibitory role for the transcription factor Stat3 in controlling IL-4 and Bcl6 expression in follicular helper T cells. J Immunol 2015;195:2080–9.
48. Rutz S, Eidenschenk C, Ouyang W. IL-22, not simply a Th17 cytokine. Immunol Rev 2013;252:116–32.
49. Chang Y, Xu L, An H, Fu Q, Chen L, Lin Z, et al. Expression of IL-4 and IL-13 predicts recurrence and survival in localized clear-cell renal cell carcinoma. Int J Clin Exp Pathol 2015;8:1594–603.
50. Wang Y, Sun SN, Liu Q, Yu YY, Guo J, Wang K, et al. Autocrine complement inhibits IL10-dependent T-cell mediated antitumor immunity to promote tumor progression. Cancer Discov 2016;6:1022.